REDUCED ORDER MODELING OF S-PARAMETER CHARACTERIZED INTERCONNECTS

BY

FRANK PETER LAMBRECHT

B.S., University of Illinois, 1997

THESIS

Submitted in partial fulfillment of the requirements
for the degree of Master of Science in Electrical Engineering
in the Graduate College of the
University of Illinois at Urbana-Champaign, 1999

Urbana, Illinois

To my family for their support

ACKNOWLEDGMENTS

I would like to thank Professor Schutt-Aine for advising the work done in this thesis. I

am grateful to Professor Klock for his encouragement. I would also like to acknowledge

that this work was partially funded by the Center for Computational Electromagentics.

TABLE OF CONTENTS

CHAPTER 1

INTRODUCTION

1.1 Overview

Since the first CPU, there has been a continuing demand for faster, more powerful processors. This demand forces designers to develop larger processors running at faster speeds. At these higher speeds, interconnects on chips connecting logic elements, bus structures, and clock trees require more accurate modeling at higher frequencies. This improved modeling will hopefully enable new designs and allow problem detection in the simulation stage of future designs. Such problems are not limited to chip design, but are also faced by system or board level designers.

1.2 Organization of Thesis

The chapters which follow address model-order reduction techniques and interconnect design. Chapter 2 reviews some of the design issues that interconnect development faces. Chapter 3 documents work in the area of S-domain reduced-order modeling. Chapter 4 covers asymptotic waveform evaluation, another method of reduced order modeling. Finally, a conclusion is given in Chapter 5.

CHAPTER 2

ELECTRICAL PERFORMANCE OF INTERCONNECTS

2.1 Performance Factors

This chapter offers a brief review of factors that influence signaling. This context should enable the reader to appreciate both the relevance of the line of inquiry that this thesis follows and the importance of this area of research.

The ability of a new interconnect system to handle higher data rates is influenced by many factors. These factors are generally classified into three areas: timing, noise issues, and electromagnetic interference (EMI). Excessive delay degrades performance when a computer architecture grows in size and complexity. The timing margin may be exceeded, resulting in loss synchronization between the data stream and the clock. Noise issues include many sources: waveform distortion along signal transmission systems, signal crosstalk, and noise in power and ground distribution systems. Simultaneous switching noise, ground bounce, and *IR* drop lead to noise issues in power and ground distribution systems. Noise coupled along ground planes and power planes due to signaling components fed by and drained to these lines is one of the most complex issues

to simulate properly. Designers often attack these problems with intuition and experimentation to combat the shortfalls of the simulator.

2.2 Clocking, Rise-Time, and Bandwidth

To understand interconnect technologies, a few rules of thumb are used to estimate signal bandwidth and rise-time when high-frequency effects become relevant. The fundamentally important relationship between bandwidth and the 10 to 90% rise-time is often approximated using

$$BW = \frac{0.35}{t_{rise}} \tag{2.1}$$

Digital interconnects are sometimes characterized with a 3-dB frequency. This corresponds to the frequency at which a 20% drop in voltage amplitude occurs. This characteristic is often used in analog systems where its usefulness is more obvious than in a digital system. A pulse will be smoothed, and the resulting rise-time will be degraded when higher frequencies are attenuated. In digital signaling, such as with 1-V emitter-coupled logic, a 15% voltage margin exists. It is therefore reasonable to consider this 3-dB margin in digital systems as well, especially when we consider that the signal will encounter other issues that cover the entire spectrum of the pulse, such as ground bounce and coupling.

When a clock rate is specified, we can use the following rule of thumb to estimate the rise-time.

$$t_{rise} = 0.07 \cdot t_{clock} = \frac{0.07}{F_{clock}} \qquad (2.2)$$

From this we can estimate the bandwidth (BW) of the clock:

$$BW_{clock} = \frac{0.35}{0.07} F_{clock} = 5F_{clock} \qquad (2.3)$$

For designs with 1-GHz clocks, we must consider the fifth harmonic when designing interconnects carrying this clock. Terminations are fundamentally important in transmission line design. These terminations are generally driver and receive circuits. There are always trade-offs when companies release technical documentation on their drivers and other circuits to promote sales. The reluctance to fully describe the drive and receive circuits results in rules of thumb like these often being used by board designers. Industry pressures have resulted in a standardization of I/O models know as input/output buffer information specification (IBIS). However these models are very simple and still leave many engineers complaining.

2.3 *Quasi-Static Approximations*

As a digital signal travels, the leading edge has a spatial and temporal description. The leading edge is spread with the spatial extent:

4

$$L_{edge} = t_{rise} \cdot v = \frac{12 in/n\sec}{\sqrt{\varepsilon_r}} \qquad (2.4)$$

This dimension is very relevant as we consider how interconnects will interact with the signal. A general rule of thumb is that when the length of interconnects is greater than half of the leading edge spatial extent, the interconnects will act like transmission lines. For very small interconnects one often limits the simulation model to a resistor-capacitor elements which accounts for the losses and delay. As an example, we can consider a 1-Ghz clock carrying line. Using the above equations we conclude that in FR-4 a length greater than 0.2-inches require transmission line modeling. Transmission lines are often referred to as long if the time required for the signal to travel to the far-end, reflect, and travel back takes longer than the rise-time.

When the spatial extent of the rise time is greater than half of the length of the interconnect, standard RLGC transmission lines provide a good model. Where the RLGC model consists of a resistor and inductor in series and a resistor and capacitor in shunt. A coupling capacitor can be added to account for the electric field coupling. In addition a mutual inductance term provides useful modeling of the magnetic coupling. These coupling values can be determined using quasi-static solvers such as the ones described in [2.1] and [2.2]. When the spatial extent of the rise-time is much less than half the length of the interconnect radiation effects become much more apparent. At this point computational field solvers provide the best model for the interconnect. Some appropriate simulation techniques for this class of interconnects are described in [2.3] and

5

[2.4]. The transfer functions generated by full-wave field solvers are often complex and do not lead to simple models. The exploration of ways to simplify these transfer functions is the general area of research into which this thesis delves.

Other important effects not fully covered in this cursory treatment of high-speed design include skin-effect and dielectric loss. Skin depth refers to the tendency of support currents to be contained in smaller cross-sectional areas as frequencies increase. This results in higher resistive losses. The frequency dependent nature of these effects contribute to difficulty in obtaining simple circuit based models for high frequency or high data rate interconnects. The high resistivity (500-1000 Ω/cm) of on-chip interconnects allow us to ignore dielectric loss, but skin effect must still be modeled. Board level designs have higher conductivity, and both effects need to be taken into account.

2.4 Delta I Noise

Another important effect that limits data rates is delta I noise. This is also referred to as simultaneous switching noise. The following equation is used to model this effect [2.5]:

$$V_{\Delta I} \cong NL_{eff} \frac{dI}{dt} \qquad (2.5)$$

The term N represents the number of switching drivers with current draw I, and L_{eff} models the inductive nature of the ground structure. Because multiple circuits simultaneously draw from the same power supply, the total current draw can be quite large. These charging currents are very short-term and are susceptible to these inductive effects. Delta I noise is worse when the rise time is the fastest and the voltage swing is the largest. The designer must be able to quantify the effect of this and understand the trade-offs. For instance, lowering the peak voltage may increase the susceptibility to thermal and crosstalk noise, but reduce delta I noise. Differential signaling can be used to combat the effects of delta I noise, at the cost of increased complexity. In a simulation variations in driver and receiver processing must be taken into account. In a typical digital design 65-70% of the driver output swing may be expected at the receiver input. This tolerance allows for DC drop and processing and power supply limitations. About 5% tolerance would be allowed for receiver switching variation. 15% is allocated to cross talk variations and 15% to Delta I noise [2.5].

2.5 References

[2.1] K. Nabors, S. Kim, and J. White, "Fast capacitance extraction of general three-dimensional structures," *IEEE Transactions on Microwave Theory and Techniques*, vol. 40, no. 7, July 1992.

[2.2] M. Karnon, M. J. Tsuk, and J. White, "FASTHENRY: A multipole accelerated 3-D inductance extraction program," *IEEE Transactions on Microwave Theory and Techniques*, vol. 42, no. 9, September 1994.

[2.3] P. Mezzanotte, M. Mongiardo, L. Roselli, R. Sorrentino, and W. Heinrich, "Analysis of packaged microwave integrated circuits by FDTD," *IEEE Transactions on Microwave Theory and Techniques*, vol. 42, no. 9, September 1994.

[2.4] J. Jin, *The Finite Method in Electromagnetics*. New York: John Wiley & Sons, 1993.

[2.5] A. Deutsch, "Electrical characteristics of interconnections for high-performance systems," *Proceedings of the IEEE*, vol. 86, no. 2, February 1998.

CHAPTER 3

REDUCED-ORDER MODEL DEVELOPMENT

3.1 Introduction

This chapter will examine reduced-order modeling of a transmission line structure using behavioral equations. These equations and their reduced-order models are relevant as we consider simulation of such transmission lines and other issues currently relevant in signal integrity modeling such as the use of computational electromagnetics. These computational methods such as finite-difference time-domain (FDTD), finite element method (FEM), and method of moments (MoM) produce transfer function descriptions of I/O relationships. Due to increased data rates in development efforts, the frequencies of interest continue to increase. At high frequencies, one must use full-wave computational formulations, which take into account radiation effects such as coupling. These formulations do not lead to simple physical coupling models as was the case in the quasi-static domain. Taking these complex transfer functions reducing their complexity while maintaining a minimum level of approximation based distortion/error is the general area in which this thesis delves.

In the research described in this thesis the problem is further limited to transmission line interconnects with equation transfer functions. Such equation-based descriptors are not generally the case in the application area described above. The general application of partial-fraction-expansion-based reduced-order modeling applies to the more general problem. The research- exploiting characteristics of the transfer function equations is less general. Another method applicable to S-parameter reduced-order modeling was shown in [3.1], which partitions the frequency and develops a reduced-order model for each frequency range.

3.2 Partial Fraction Iterative Algorithm

The transfer function for transmission lines can be approximated using partial fraction expansions or pole-residue models. This simplifies inversion to the time domain. The following iterative algorithm can be used to generate such a model. The equation $g(w)=\text{Real}[e^{-\gamma l}]$ can be approximated using the following expansion:

$$g(w) \cong A + \sum_{i=1}^{L} \frac{a_i}{1 + \dfrac{w^2}{w_{ci}^2}} \tag{3.1}$$

The following relationship enables transform to the time domain:

$$\frac{2a}{a^2 + \omega^2} \Leftrightarrow e^{-a|t|} \tag{3.2}$$

The output from such a transfer function can then be determined using recursive convolution with the sum of exponentials described above.

3.3 Transfer Function Approximations

The transfer function of a transmission line (TL) includes periodic behavior. This is displayed in Figure 3.1. In this plot, Real[$e^{-\gamma l}$] is plotted versus frequency($R = 1$ $G = 1$ $L/\omega_{max} = 20/8$ $C/\omega_{max} = 1/8$). Initially, there is asymptotic behavior, then the function follows:

$$\text{Real}\left[e^{-\gamma L}\right] \rightarrow e^{-j\omega\sqrt{LC}} \quad \text{as} \quad \omega \rightarrow \infty \tag{3.3}$$
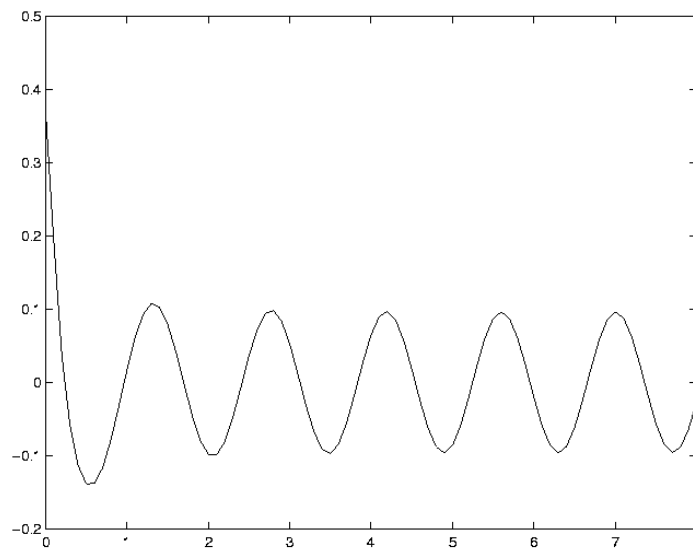

Figure 3.1 Transmission line transfer function versus frequency.

Such periodic behavior is not well suited to approximation by Equation (3.1). When we multiply $e^{-\gamma l}$ by $e^{-j\,\omega\,sqrt(LC)}$ this periodic behavior is removed. To demonstrate this, a plot of Real[$e^{-\gamma l}\,e^{-j\,sqrt(LC)}$] versus frequency is shown in Figure 3.2. Multiplication by $e^{-j\,\omega\,sqrt(LC)}$ presumes knowledge of *L* and *C* or the ability to extract these parameters from a transfer function. The factor of $e^{-j\,\omega\,sqrt(LC)}$ allows use of the shift property of the Fourier transform:

$$f(t - \sqrt{LC}\;) \leftrightarrow F(\omega)e^{-j\omega\sqrt{LC}} \qquad\qquad (3.4)$$
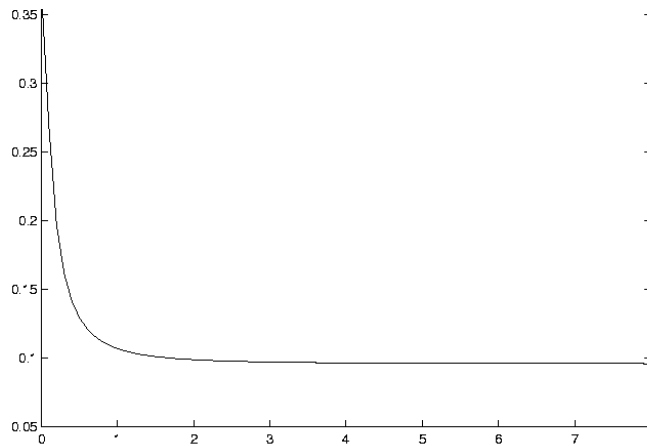

Figure 3.2 Approximation to transfer function versus frequency.

We can transform our approximation to the time domain, and apply the shift property to

obtain an approximation of the time domain response. It should be stressed that the

multiplication of $e^{-\gamma l}$ by $e^{-j\,\omega\,sqrt(LC)}$ is valid for high frequencies. Multiplying by this

factor introduces error, especially at low frequencies. The benefit of this method is that

we do not need to reduce our model to the lossless case in order to improve the

computational efficiency for a SPICE simulator.

3.4 Partial Fraction Iterative Algorithm Development

The a_i and ω_{ci} terms in Equation 1 can be determined using the following algorithm.

It should be noted that these terms could also be solved for through matrix inversion, as

has been demonstrated in various forms [3.2]. One benefit of the iterative method is that

it avoids the problems that may arise due to ill-conditioned or sparse matrices in this

application.

The first step in the algorithm is to choose $2L + 1$ frequency points, where L is the

number of elements in the summation of Equation (3.5). In the work done in this

research $f=f_{max}[i/2L]^7$ was used to determine the frequencies used. Initially the variables

were set as $a_i=0$ and $\omega_{ci}=1$. The following equations were used to updates these

variables:

$$\psi_{2i} = \sum_{\substack{j=1 \\ j\neq i}}^{L} \frac{a_i}{1+\dfrac{\omega_{2i}^2}{\omega_{cj}^2}} \qquad\qquad (3.5)$$

13

$$\psi_{2i-1} = \sum_{\substack{j=1 \\ j\neq i}}^{L} \frac{a_j}{1 + \dfrac{\omega_{2i-1}^2}{\omega_{cj}^2}} \tag{3.6}$$

$$\theta(\omega_{2i}) = g(2i) - \psi_{2i} - A \tag{3.7}$$

$$\theta(\omega_{2i-1}) = g(2i-1) - \psi_{2i-1} - A \tag{3.8}$$

Where A is defined as the following:

$$A = g(0) - \sum_{j=1}^{L} a_j \tag{3.9}$$

The constant A is the dc response of the system at each step of the iteration.

$$\omega_{cj}^2 = \frac{\theta_i(\omega_{2i})\omega_{2i}^2 - \theta_i(\omega_{2i-1})\omega_{2i-1}^2}{\theta_i(\omega_{2i-1}) - \theta_i(\omega_{2i})} \tag{3.10}$$

In these equations $g(f)$ is the original function we are approximating.

14

The derivation of these equations is quite straightforward and is demonstrated in the following steps. Equations (3.7) and (3.8) defined above provide the following quantities:

$$\theta\left(\omega_{2i}\right) = \frac{a_i}{1 + \dfrac{\omega_{2i}^2}{\omega_{cj}^2}} \tag{3.11}$$

$$\theta\left(\omega_{2i-1}\right) = \frac{a_i}{1 + \dfrac{\omega_{2i-1}^2}{\omega_{cj}^2}} \tag{3.12}$$

By equating the values for a_i we can solve for w_{cj} obtaining Equation (3.10) above. We can then use this solution for w_{cj} to find a_i using Equation (3.11) or (3.12).

3.5 Application of Algorithm to S-Parameters

Given a transfer function $X = e^{-\gamma l}$ for a transmission line and terminations for that transmission line, we can generate an S-parameter model using the equations given below. We will then consider methods to simplify this S-parameter model for more computationally efficient use in a time domain simulator. The system shown in Figure 3.3 was considered. This corresponds to a system that has a potentially lossy transmission line structure embedded in a reference system. This could be a model used

for a signal line connecting a driver and receiver that have approximately the same input
and output impedance. In timing and signal integrity analysis this is often the case. The
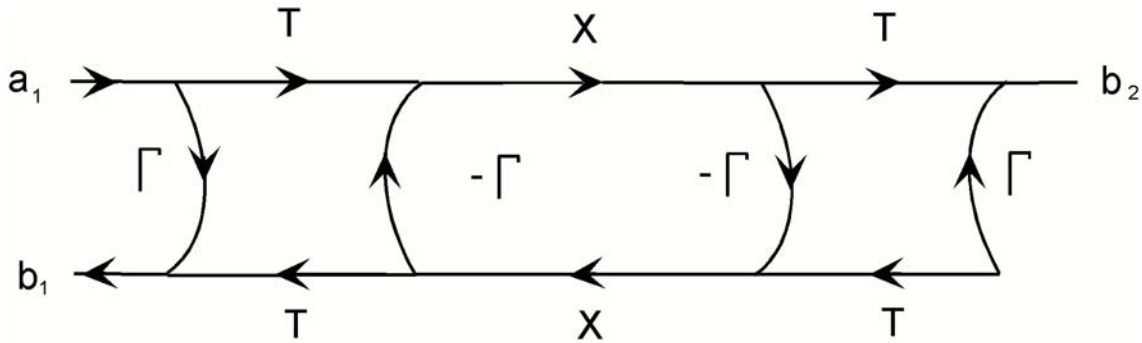impedance may be as simple as a shunt capacitive load.

Figure 3.3 Transmission line flow graph.

Applying Mason's rule or tiling of S-parameters to this signal flow diagram yields the
following relationship:

$$S_{11} = \frac{\Gamma\left(1 - X^2\Gamma^2\right) - \Gamma T^2 X^2}{1 - \Gamma^2 X^2}$$
(3.13)

Equation (3.13) can be simplified to the following when we consider $\Gamma^2 + T^2 = 1$ since the
reference system is lossless:

$$S_{11} = \frac{(1 - X^2)\Gamma}{1 - \Gamma^2 X^2} \tag{3.14}$$

We can also obtain a formula for the resultant S_{21} using Mason's rule.

$$S_{21} = \frac{T^2 X}{1 - \Gamma^2 X^2} \tag{3.15}$$

If we apply $\Gamma^2 + T^2 = 1$ once more, we obtain the following:

$$S_{21} = \frac{(1 - \Gamma^2)X}{1 - \Gamma^2 X^2} \tag{3.16}$$

where

$$X = e^{-\gamma L} \tag{3.17}$$

The term Γ is the reflection coefficient looking in to the transmission line. This is calculated using the following:

$$\Gamma = \frac{\sqrt{\dfrac{R + j\omega L}{G + j\omega C}} - \sqrt{\dfrac{L}{C}}}{\sqrt{\dfrac{R + j\omega L}{G + j\omega C}} + \sqrt{\dfrac{L}{C}}} \tag{3.18}$$

As the characteristic impedance of sqrt(L/C) was chosen to minimize the reflection coefficient at higher frequencies. This can also be expressed in the following limit.

$$\lim_{\omega \xrightarrow{\quad} \infty} \Gamma = 0$$

(3.19)

As in Section 1.2 we want to reduce periodicity. In this case we want to reduce the periodicity of the S-parameters in order to make them more easily approximated by partial fraction expansions or other simplified models. This is demonstrated in Figure 3.4. The reduced model development is shown in Equation (3.20) and (3.21).
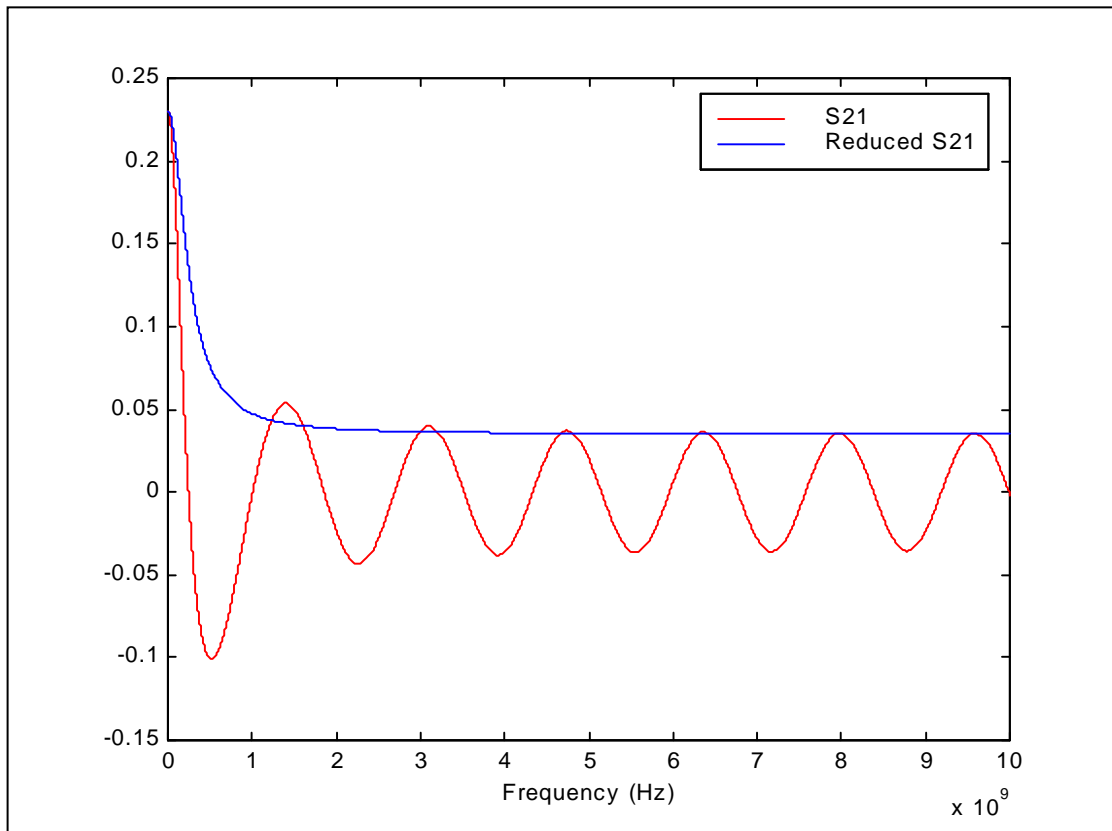

Figure 3.4 S_{21} and reduced S_{21} versus frequency.

$$S_{21}' = S_{21}X_o^{-1} \tag{3.20}$$

where

$$X_o^{-1} = e^{-j\beta L} \tag{3.21}$$

In Section 2.4 a partial fraction iterative algorithm was discussed which can now be applied to the simplified S_{21}. With five terms in the series given in Equation (3.5) and using the algorithm decribed in Section 2.4 running through five iterations, Figure 3.5 was generated. As can be seen, the partial fraction expansion-based approximation is virtually indistinguishable from the original function.

We next consider approximations for S_{11}. In what follows in this section and the next few sections are various methods that attempt to reduce the asymptotic periodicity of S_{11}. If in Equation (3.14) we approximate the $(1 - X^2)$ factor with the expression for the lossless case: $X = e^{-j\beta l}$ the following equation results:

$$\frac{S_{11}}{\beta l} \cong \frac{\Gamma}{\left(1 - \Gamma^2 X^2\right)} \frac{2 j \sin c(\beta l)}{e^{j\beta l}} \tag{3.22}$$

The remaining terms in the approximation all account for a lossy system. The following approximation was considered.

19

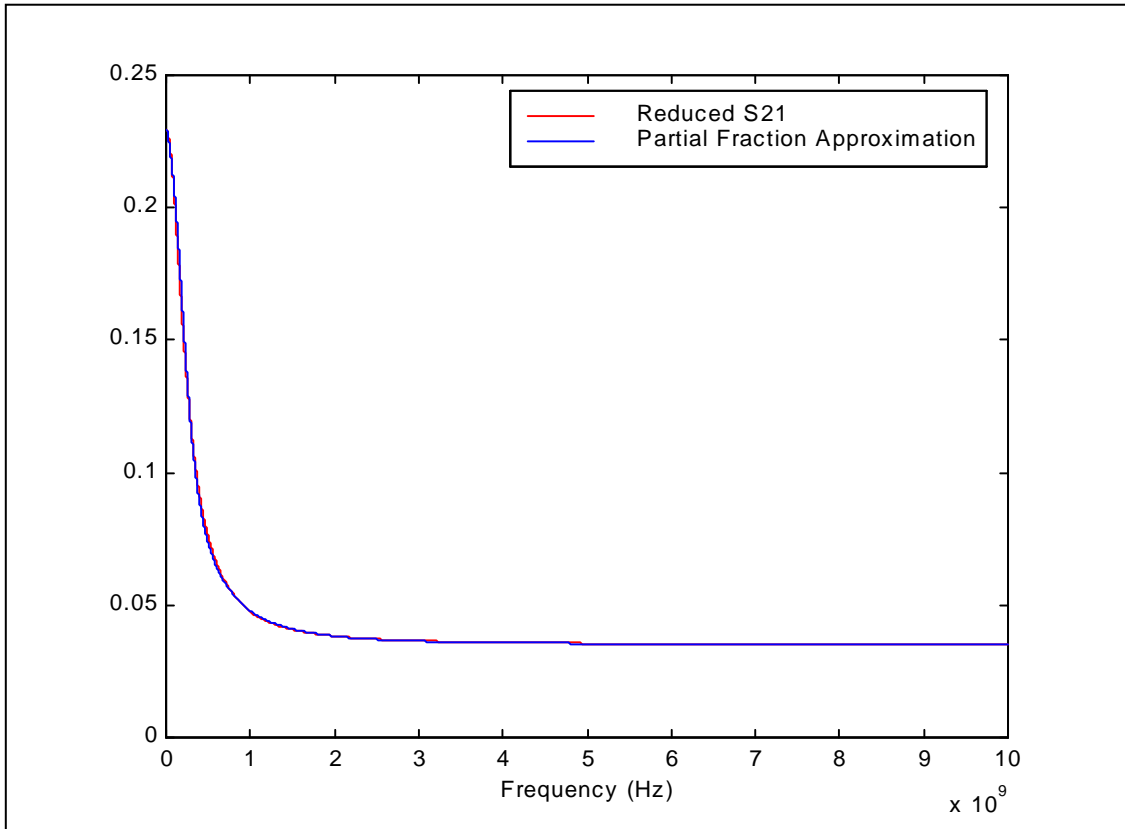$$S_{11}' = \frac{S_{11}}{2 \, je^{+j\beta L} \text{sinc}(\beta L)} \tag{3.23}$$

Figure 3.5 Reduced S_{21} and partial fraction approximation versus frequency.

We want to see if this would reduce the effect of the sinc(βl) term, thereby counteracting the impact of the $(1-X^2)$ term in the numerator of Equation (3.14). If Γ is sufficiently small, then the periodicity caused by the denominator will be much less than that of the numerator in Equation (3.14). Unfortunately use of the sinc(βl) term causes singularities when used in a lossy system as is shown in Figure 3.6.
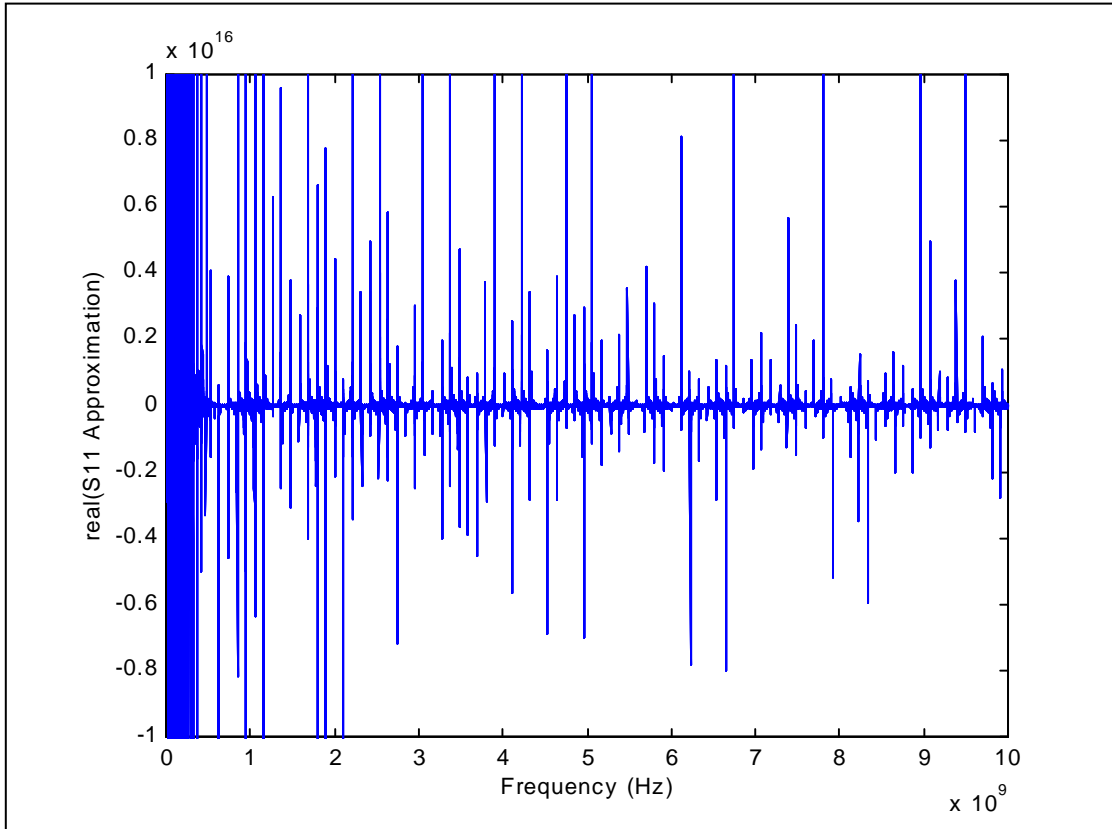
Figure 3.6 Real component of S_{11} approximation versus frequency.

The plot shown in Figure 3.6 is an approximation to the S_{11} curve shown in Figure 3.7. This was generated for a nearly lossless case where $R = .0001\ \Omega$, $G = .2\ \Omega^{-1}$, $L = 418$ nH, and $C = 93$ pF.

3.6 Clipped Cotangent Function Based Approximation

21

The relationship below can be derived from Equation (3.14) above assuming a lossless transmission line,
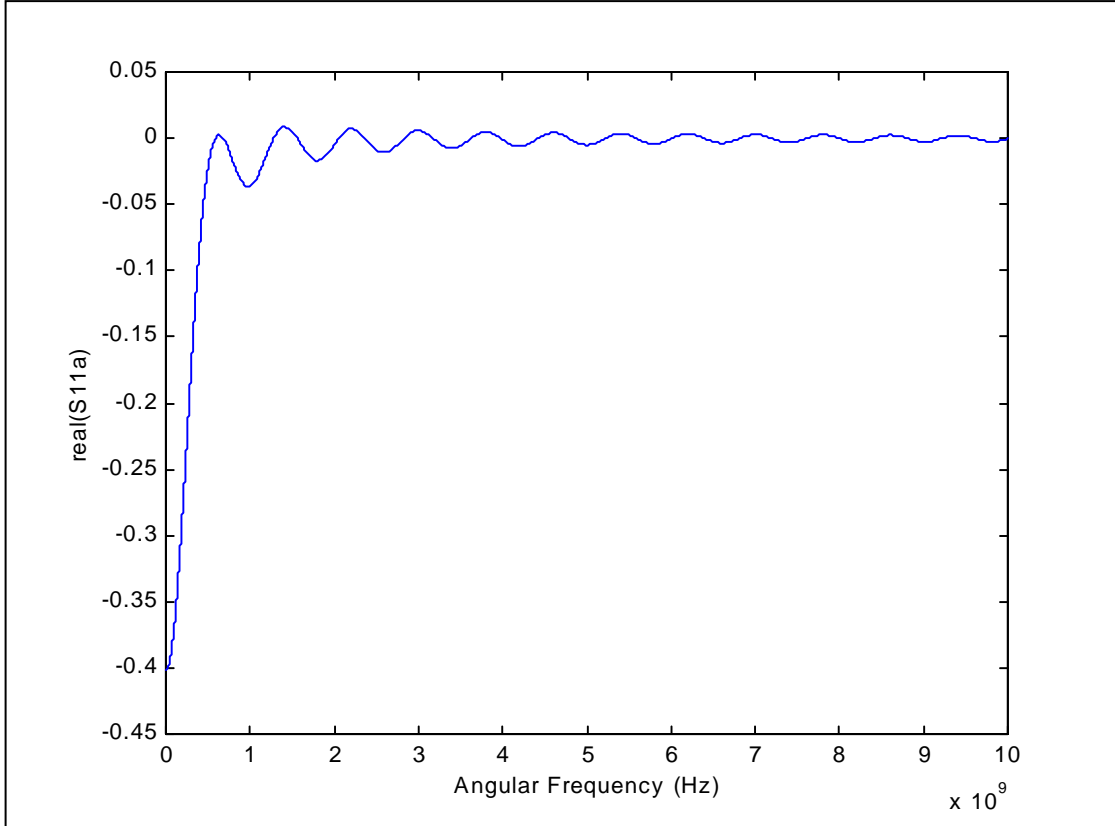

Figure 3.7 Real component of S_{11} versus frequency.

$$S_{11} = \frac{\Gamma(2j\sin(\beta l))}{e^{j\beta l}(1 - X^2\Gamma^2)} = \frac{\Gamma}{(1 - X^2\Gamma^2)} \frac{2j\sin(\beta l)}{(\cos(\beta l) + j\sin(\beta l))} \tag{3.24}$$

We can multiply S_{11} by the following

$$\frac{(\cos(\beta l) + j\sin(\beta l))}{2j\sin(\beta l)} = 0.5(1 + j\cot(\beta l)) \tag{3.25}$$

22

For a lossless S_{11} this would cancel one term which causes asymptotically periodic behavior. Small numerical inaccuracies could lead to infinite S_{11} values, due to the cotangent term. If we want to apply this to the case of lossy transmission lines we are almost guaranteed to run into this problem. A logical conclusion might be to limit the maximum values the cotangent introduces. This is shown in Figure 3.8 below.
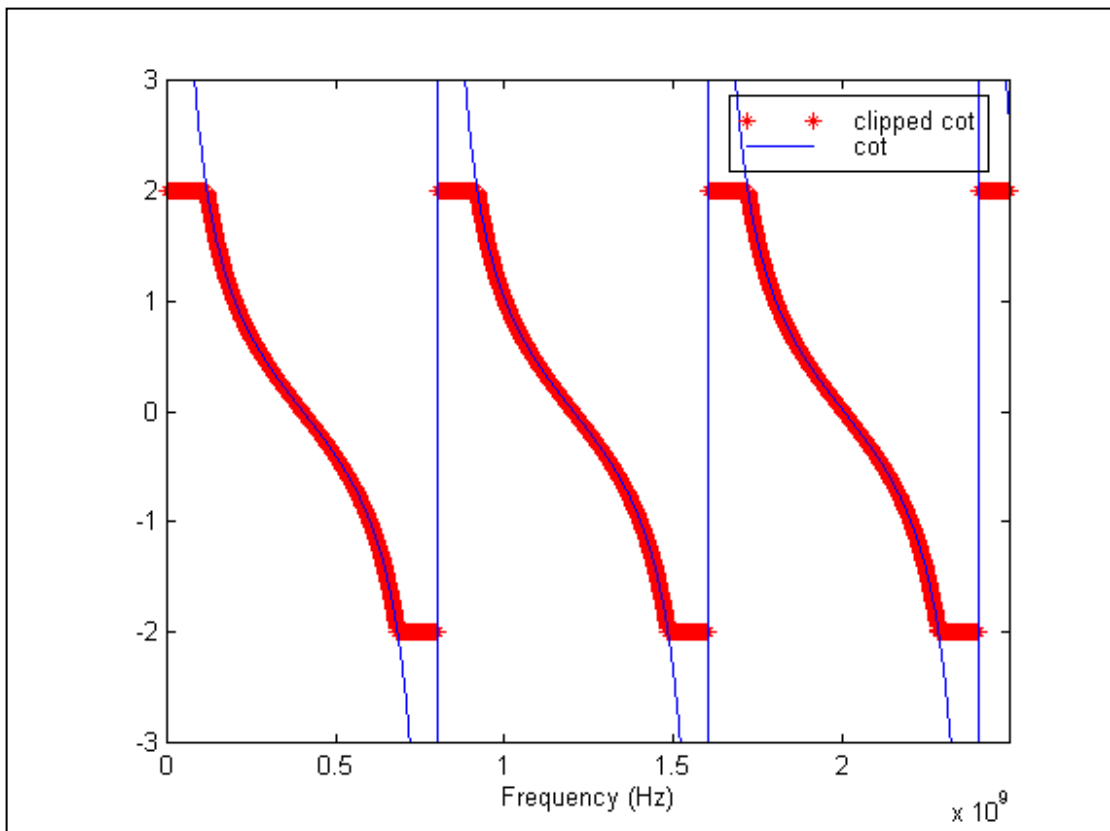
Figure 3.8 Cotangent and clipped cotangent versus frequency.

A modified transfer function using this method is plotted in Figure 3.9 for a lossless transmission line. It can be seen that this method does successfully reduce the periodic

behavior. For the case of a lossless transmission line, we also do not need to limit the

values the cotangent function can take.
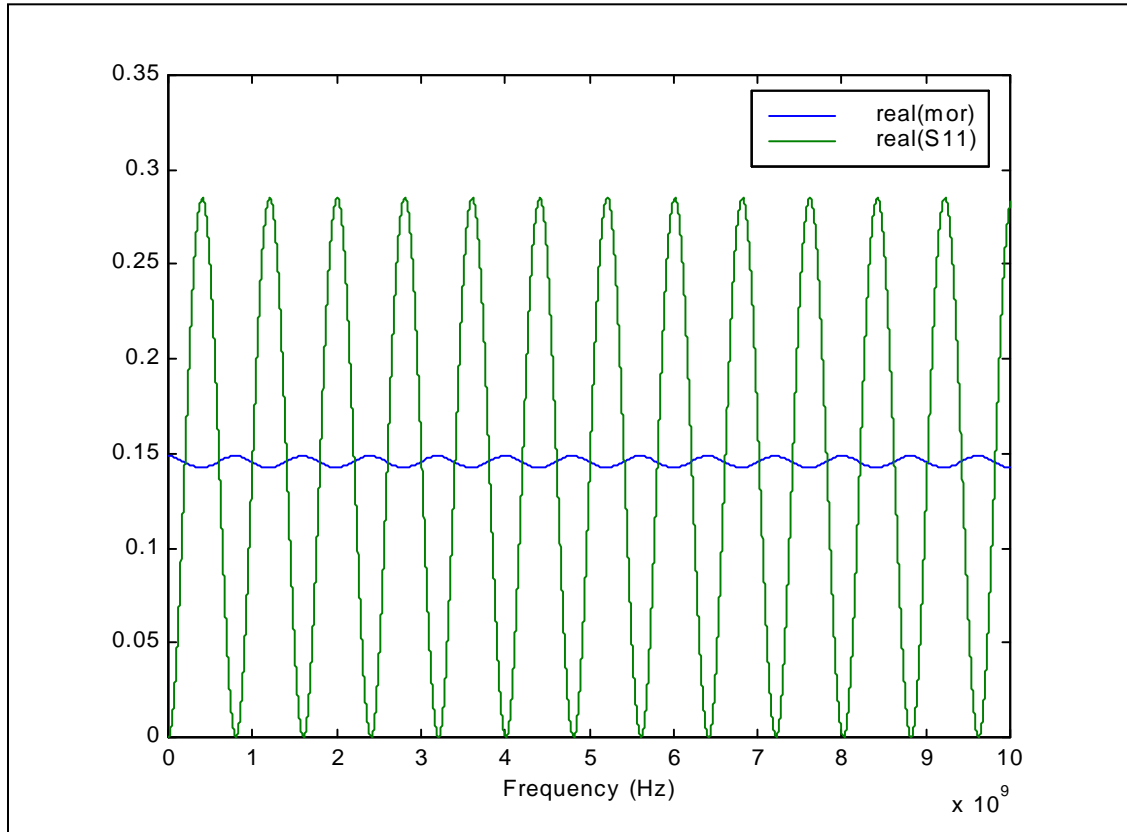
Figure 3.9 Lossless S_{11} and reduced lossless S_{11} versus frequency.

When we consider a lossy transmission line the goal of reducing the periodic

behavior is not met as demonstrated in Figure 3.10. This is at least partially because the

periodic behavior of a lossy line does not have the same resultant periodicity as a lossless

line. Also the values taken at the minimum of this quasi-periodicity are not zero, unlike

for the lossless case.
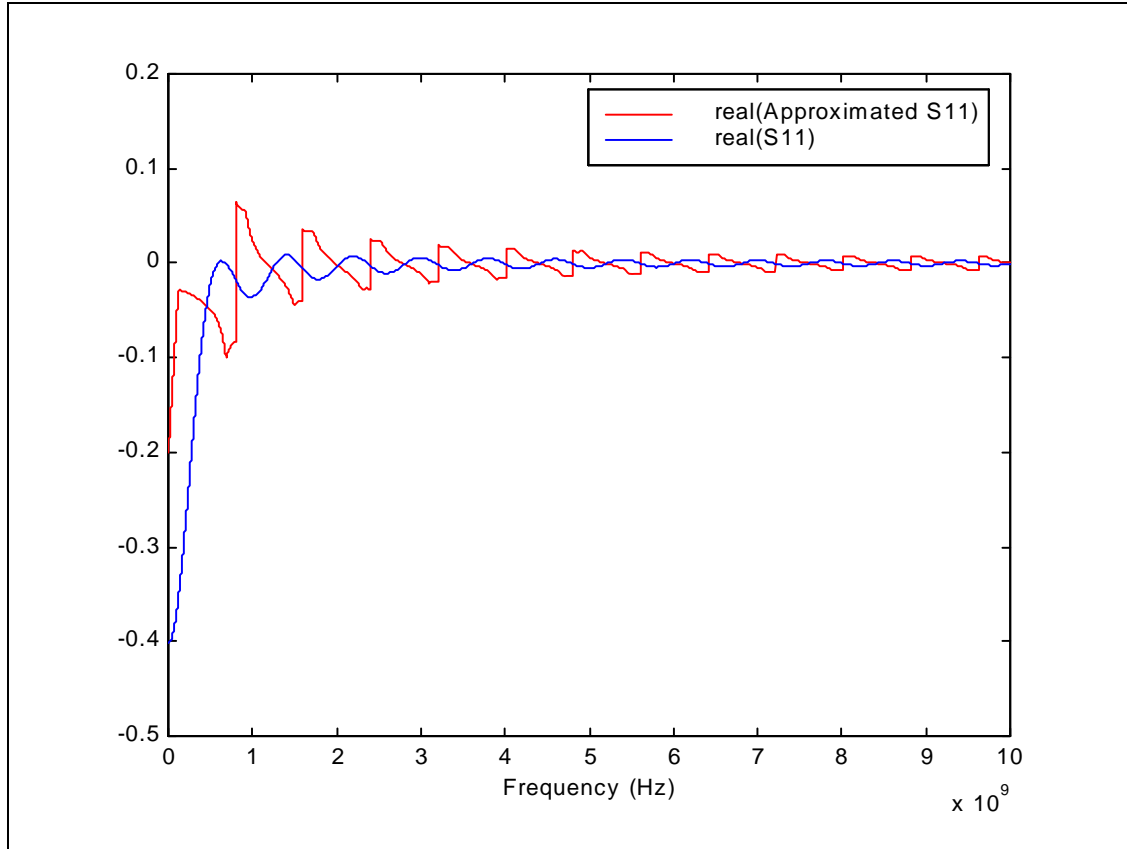
Figure 3.10 Real component of S_{11} and approximated S_{11} versus frequency.

3.7 Geometric Series Approximation

Equation (3.14) can be recast as a geometric series approximation:

$$S_{11} = \frac{(1-X^2)\Gamma}{1-\Gamma^2 X^2} = (1-X^2)\Gamma \sum_{k=0}^{\infty} \left(\Gamma^2 X^2\right)^k \qquad (3.26)$$

For the S_{11} curve considered earlier, Figure 3.7, it takes only two terms in the summation to provide a good approximation. This is shown in the Figure 3.11, and was also found to generally be the case.

Figure 3.11 Real component of S_{11} and two approximations versus frequency.

The term Γ is a constant in the quasi-static approximation where characteristic impedance is constant. The factor $\Gamma^2 X^2$ can then be approximated using lossless transmission line conditions that allow us to use the shift property of the Fourier transform described in Equation (3.4) to simplify inversion to the time domain.

By inspection we can see that Equation (3.26) corresponds to the following in the time domain:

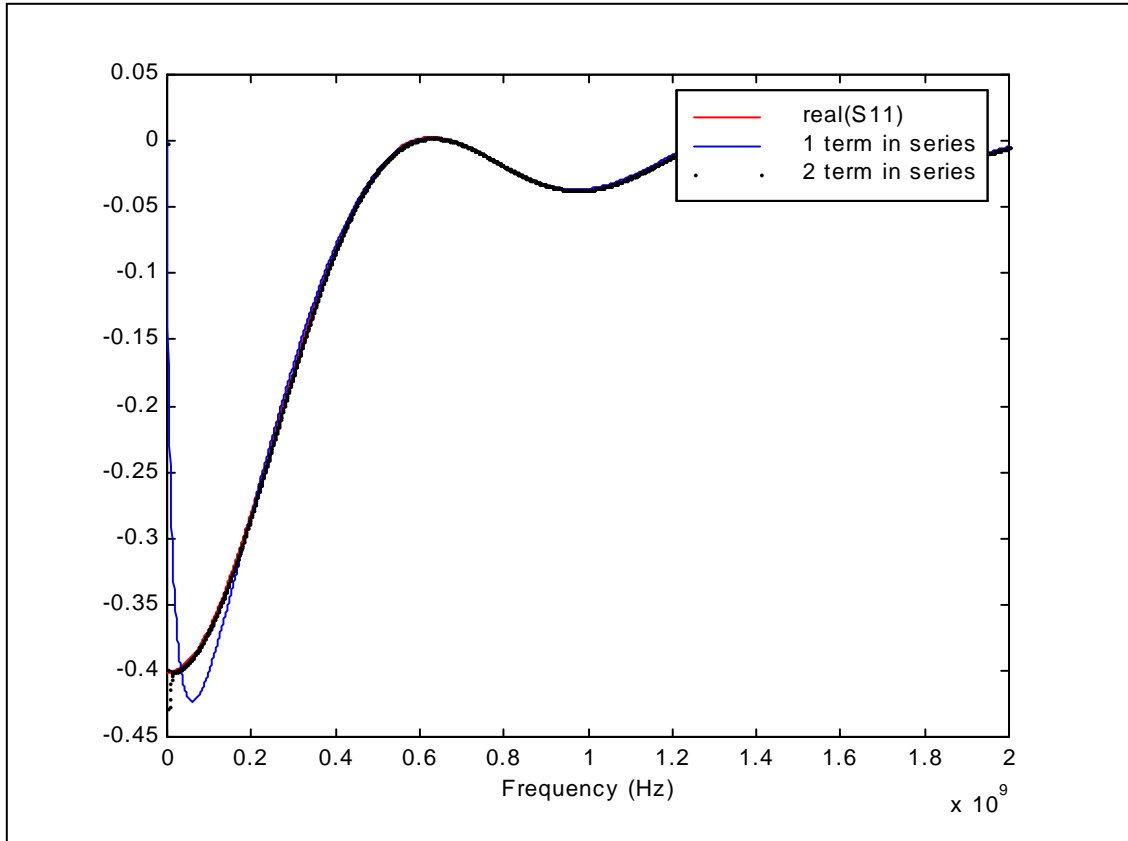$$S_{11} \leftrightarrow \left(\partial(t) - F^{-1}\left(X^2\right) \right) \Gamma \sum_{k=0}^{\infty} \left(\Gamma^2 F^{-1}\left(X^2\right) \right)^k \qquad (3.27)$$

As an approximation we can use the lossless *X* again. In a marching-on-time based simulator, a convolution would occur with this transfer function to determine the backward-travelling pulse. As long as Γ is sufficiently small, the effect of neglecting loss in the transfer function *X* could be negligible, and computation cost could be saved by using the shift property once more. This time applying it to the first term in Equation (3.27). This method was found to produce erroneous transfer functions in some cases. This method can be applied in some cases and a variation of this method may prove to be suitable for general usage.

3.8 References

[3.1] M. Silviera, I. Elfadel, J. White, M. Chilukuri, and K. Kenneth, "Efficient frequency-domain modeling and circuit simulation of transmission lines," *IEEE Transactions on Components, Hybrids, and Manufacturing Technology-Part B*, vol. 17, no. 4, November 1994

[3.2] W. T. Beyene and J. E. Schutt-Aine, "Model-order reduction techniques for circuits and interconnects simulation," University of Illinois Electromagnetics Laboratory Scientific Report No. 97-1, February 1997.

CHAPTER 4

ASYMPTOTIC WAVEFORM EVALUATION

4.1 Introduction

Asymptotic waveform evaluation (AWE) is a simulation method well suited for time-delay analysis at a chip and board level. This chapter will give an overview of AWE and models that are used in this analysis. AWE is a form of Padé approximation, which uses moment matching to determine the dominant poles and zeroes of a network. AWE has been used to enable fast frequency sweep capability to commercial FEM tools since 1993 [4.1]. Asymptotic waveform evaluation is so named because the approximation generated approaches the response of the original function asymptotically with time.

The Padé approximation is accomplished by matching the first $2q$ coefficients of the Maclauren series expansion of the actual transfer function with a reduced order model of order q. This approximation is used because for many large, physical systems, it is easier to obtain the series expansion than a closed form solution of the transfer function [4.2]. The AWE approximation generally involves an approximation at zero and

infinite frequencies. To increase accuracy at frequencies of interest, the method of

complex frequency hopping (CFH) was developed, which involves hopping to multiple

points for expansions. CFH is well documented in [4.3] and [4.4].

This chapter will first look at a state space formulation of the AWE

approximation. Then the modified nodal admittance (MNA) matrix will be considered

and applied to a formulation applicable to uniform lossy coupled transmission lines will

be considered. Stability issues will be discussed as well as a methodology for increasing

the stability of AWE. CFH will be considered as an efficient means of increasing the

accuracy of the AWE approximation. Lastly, some limitations of AWE will be noted.

4.2 State Space Formulation of AWE Approximations

The AWE approximation can be most easily described in terms of a state space

formulation [4.2].   Another formulation is the modified nodal admittance formulation.

This method is described in the next section. The differential state equation for a lumped,

linear, time invariant circuit is:

$$\dot{x} = Ax + Bu \qquad (4.1)$$

The term x is an n-dimensional state vector. Given a pulse excitation

$$u_p(t) = u_o + u_1 t \qquad (4.2)$$

29

Where the u's are m-dimensional vectors. A particular solution to this differential state equation can be found. This procedure is not limited to pulse excitation but can be applied to other inputs. For the pulse excitation the differential state equation is satisfied by the following equation:

$$x_p(t) = -A^{-1}Bu_o - A^{-2}Bu_1 \qquad (4.3)$$

If we limit the state equation to the homogenous form, $Bu = 0$ and we can easily show that the Laplace Transform of the homogeneous form is given by

$$X_h(s) = (sI - A)^{-1}x_h(0) \qquad (4.4)$$

Where x_h can be derived from the solution to the unhomogeneous differential state equation by setting $t = 0$. To begin approximating this function we expand $X_h(s)$ in a Maclauren series. This takes the form of

$$X_h(s) = -A^{-1}(I + A^{-1}s + A^{-2}s^2 + \ldots\ldots)x_h(0) \qquad (4.5)$$

The coefficients of the powers of s are often referred to as the moments. These will be used to approximate the expansion by a lower-order model. The method of moment matching is loosely based upon the Laplace transform.

$$X(s) = \int_0^\infty e^{-st} v(t) = \sum_{k=0}^\infty \frac{(-s)^k}{k!} \int_0^\infty t^k x(t) dt \qquad (4.6)$$

Where the moments follow as

$$m_k = \frac{(-1)^k}{k!} \int_0^\infty t^k x(t) dt \qquad (4.7)$$

Where it is interesting to note that $X'(0) = -T_d$, which is the Elmore delay. The Elmore expression is a method of approximating the time delay for a step response to reach 50 % of its final value, which is used in timing analysis for lower frequency circuits. It is useful to have the transfer function expressed in the form

$$H(s) = c + \sum_i \frac{k_i}{s - p_i} \qquad (4.8)$$

This allows simple transform to the time domain using the properties of the Laplace transform. For example, the time domain response due to a single pole is

31

$$L^{-1}\frac{K}{s-p}=Ke^{pt} \tag{4.9}$$

Expressions for Laplace tranforms of multiple poles, and complex conjugate poles also exist and aid in a simple transform to the time domain. This then allows the time domain impulse response to be represented in the form of a partial fraction expansion:

$$h(t)=c\partial(t)+\sum_{j=1}^{q}k_{j}e^{p_{j}t} \tag{4.10}$$

This time domain representation enables the inclusion of the interconnect model in a network that includes both linear and nonlinear elements. In a complex interconnect system, such as with VLSI, a signal passes through many levels of interconnects, including on-chip, packaging, and board-level interconnects. These all must be taken into account, and they all will increase the complexity of the structure. These interconnects can often be modeled with passive distributed circuit models; however, the time domain models cannot. Therefore, time-domain modeling must always be addressed when developing an interconnect modeling system.

To determine the poles and zeroes of the approximating function, one can expand each of the terms of the partial fraction expansion in a series about the origin. For each element in the vector x, this expansion yields a set of equations of the form

$$-\left(\frac{k_{1}}{p_{1}^{i}}+\frac{k_{2}}{p_{2}^{i}}+...+\frac{k_{q}}{p_{q}^{i}}\right)=m_{i} \tag{4.11}$$

32

For each element in the vector x, this expansion can then be expressed in the matrix equation

$$-Vk = m_i \qquad (4.12)$$

and

$$V\Lambda^{-q}k = m_i \qquad (4.13)$$

The matrix $\mathbf{V}$ is the Vandermonde matrix, and the matrix Λ^{-1} is a diagonal matrix of the reciprocals of the poles. The Vandermonde matrix is shown in Equation (4.14):

$$V = \begin{bmatrix} 1 & 1 & \cdots & 1 \\ p_1^{-1} & p_2^{-1} & \cdots & p_q^{-1} \\ \vdots & \vdots & & \vdots \\ p_1^{-q+1} & p_2^{-q+1} & \cdots & p_q^{-q+1} \end{bmatrix} \qquad (4.14)$$

The nature of the Vandermonde matrix makes it ill-conditioned. This is especially true for large poles. Another significant problem is that the Vandermonde matrix is singular for repeated roots. A generalized approach to dealing with r-order repeated roots is given in [4.2].

What remains in the formualtion of the AWE problem is to solve for the poles and zeroes. The zeroes can be obtained by a matrix inversion and multiplication. To find the poles, the zeroes are used along with further matrix manipulation detailed in [4.3] and [4.4]. An improvement upon the Padé approximation described above can be made by including an approximation about s = infinity. Using a Laurent series to approximate the transfer function is documented in [4.4] and [4.8].

4.3 MNA Formulation of AWE

In order to consider the application of AWE to uniform lossy-coupled transmission lines, we will first consider the MNA formulation of a linear subnetwork. This formulation can be found with more detail in [4.4] and [4.6]. If we consider a subnetwork that contains N_t transmission lines, and n_k coupled conductors in transmission line set k. There are N nodal variables internal to the subnetwork. The MNA matrix can then be formulated as

$$C \ \frac{d}{dt}v \ (t) + Gv(t) + \sum_{k=1}^{N_t} D_k i_k (t) - e(t) = 0 \qquad (4.15)$$

Where $v(t)$ is the vector describing the subnetwork which include node voltages waveforms appended by independent voltage source current, linear inductor current, nonlinear capacitor charge and nonlinear inductor flux waveforms. The term C is a matrix that describes the memory elements of the network. The term G is a matrix containing the memoryless elements. The function $e(t)$ describes the vector of source

waveforms. The term $D_k = [d_{i,j}]$ with elements di,j which equal zero or one, $i = \{1, 2, 3,$

...., $N\}, j = \{1, 2, ..., 2n_k \}$. The matrix D_k has a maximum of one nonzero element in

each row or column. This matrix maps the currents entering the subnetwork to the node

space of the network.

If there are no transmission lines in the network, then the formulation can be

reduced to three terms by dropping the summation term. To represent the frequency

domain equation of the transmission line subnetwork in a general way, we use the

following:

$$A_k V_k(s) + B_k I_k(s) = 0$$
$$(1 \le k \le N_t)$$

(4.16)

Taking the Laplace Transform of the MNA matrix equation and the using the expression

above leads to the following matrix equation:

$$\begin{bmatrix} sC+G & G & \cdots & & D_{N_t} \\ A_1 D_1^T & B_1 & 0 & \cdots & 0 \\ \vdots & & \ddots & & \vdots \\ A_N D_N^T & 0 & 0 & & B_{N_t} \end{bmatrix} \begin{bmatrix} V(s) \\ I_1(s) \\ \vdots \\ I_{N_t}(s) \end{bmatrix} = \begin{bmatrix} E \\ 0 \\ \vdots \\ 0 \end{bmatrix}$$

(4.17)

Or

$$\overline{Y}(s)\overline{V}(s) = \overline{E}$$

(4.18)

When there no distributed components Equation (4.18) reduces to

$$|G + sC| = 0 \tag{4.19}$$

It is interesting to note that the solution to the matrix equation is described by all values that satisfy

$$\left|\overline{Y}(s)\right| = 0 \tag{4.20}$$

From Equation (4.20), one can see how the number of poles could become very large as the *Y* matrix grows. Therefore, the AWE approximation can be used to find the lower-order poles in a very complex system. As in the previous section on the state space formulation, the matrix equation can be expanded in a Maclauren series to produce a reduced order model this formulation is shown in [4.4].

4.4 Application of AWE to Lossy Coupled Transmission Lines

Lossy-coupled transmission lines are often modeled through use of the telegrapher's equations. In the *S*-domain the telegrapher's equations can be combined to produce

$$\frac{\partial^2}{\partial x^2} V(x) = -Z_p Y_p V(x)$$

$$\frac{\partial^2}{\partial x^2} I(x) = -Y_p Z_p I(x)$$

(4.21)

Where $Z_p = R + sL$ and $Y_p = G + sC$. The terms R, S, L, C are all matrices where the diagonal elements describe selfvalues, and the off diagonal elements at location i, j represent the mutual values between transmission line i and j.

To perform the AWE approximation, one needs an expansion of the s-domain telegrapher's equation. The main concern remains in finding the most computationally efficient method to produce this expansion. In [4.4] and [4.6], modal expansions were considered. These involve describing the transfer in the following manner:

$$A(s)\begin{bmatrix} V(0,s) \\ V(d,s) \end{bmatrix} + B(s)\begin{bmatrix} I(0,s) \\ I(d,s) \end{bmatrix} = 0$$

(4.22)

This method exploits the fact that the solution for the modal voltages and currents are of the form

$$V_m(x) = V_m(0)e^{\pm \gamma_m x}$$

$$I_m(x) = I_m(0)e^{\pm \gamma_m x}$$

(4.23)

These can be substituted into the telegrapher's equations above to obtain the following:

37

$$\gamma_m^2 I - Z_p Y_p = 0 \tag{4.24}$$

The details of this analysis are rather long and involved, so the reader should see [4.4] and [4.6] for the details and the final solution. One efficient aspect of this method is that a recursive scheme can be applied to determine the necessary derivatives. This significantly increases the efficiency of this method.

4.5 Improvements upon the Basic AWE Algorithm and Stability Issues

Within the AWE method one must be concerned with two types of instability: numerical and inherent. Numercal instability may occur when the frequency range of interest compels the model to include higher frequency poles. Inclusion of these higher-frequency poles results in numerical issues, such as ill conditioning. It is easy to see that the Vandermonde matrix becomes ill conditioned as the poles become larger. Within computer precision large poles could result in singular matrices. Singular matrices prevent the algorithms presented above from being used since they all depend upon matrix inversion.

Large magnitude poles typically do not have large influence on the response of interconnects. However these large-order poles do affect the accuracy of the lower-order moments. This is referred to as an *inherent instability*. This effect is interpreted as noise in the lower order moments and can at times cause unstable AWE approximations.

Anastasakis et al. [4.7] suggest an improvement on the basic AWE method to increase stability and accuracy of interconnect models when the signal includes higher-frequency components. They suggest that the poles included in an approximation should be limited by considering the frequency of the excitation. If the majority of the power in a signal is contained below a certain frequency, the AWE approximation could be limited to include only the frequency range of interest. They also suggest a reformulation of the moment equations. If one considers the Laplace transform of a step input: s or a ramp s^{-2}. The S-domain response of an interconnect circuit can be obtained by multiplying the transfer function by the Laplace transform of the input. The response due to a ramp can be considered as follows:

$$R_{ramp}(s) = \frac{m_o}{s^2} + \frac{m_1}{s} + m_2 + m_3 s + ... \tag{4.25}$$

If one considers the moment matching technique applied to this or generalized to a Laplace domain function of p^{-j}, then the moment matching equation for the $i + j$ moment is as follows ($i = 0, 1, 2, \ldots$):

$$-\left(\frac{k_1^{'}}{p^{i+1}} + \frac{k_2^{'}}{p^{i+1}} + ... \right) = m_{i+j} \tag{4.26}$$

Where the new residues related to the residues of H(s) are as follows ($r = 1, 2, 3, \ldots$):

$$k_r^{'} = \frac{k_r}{p_r^{j}} \tag{4.27}$$

This new formulation retains the same poles but the residues are changed. Further the larger poles will correspondingly reduce in magnitude by a greater factor than the smaller poles. This general method can also be likened to a shifting of the approximation to a lower-frequency model. As was described above, the lower-frequency models tend to be more stable than the higher-frequency counterparts.

4.6 Complex Frequency Hopping

The complex frequency hopping (CFH) algorithm is based upon the fact that Padé approximations are most accurate near the point of expansion. This method is well documented in [4.3]. The method involves forming Taylor expansions about frequency points such as $p = a + jb$ rather than zero or infinity, as was considered above. This will result in a new approximation given below:

$$H(s) = m_0^{'} + m_1^{'}(s - p) + m_2^{'}(s - p)^2 \tag{4.28}$$

One could then follow a similar approach as above in determining the matrix equation formulations. The authors of [4.3] maintain that this is not the best way to perform CFH. They describe a new formulation based upon the following:

$$\Phi(x, s) = e^{(A+sB)d} \Phi(0, s)$$

$$A = \begin{bmatrix} 0 & -R \\ -G & 0 \end{bmatrix}$$

$$B = \begin{bmatrix} 0 & -L \\ -C & 0 \end{bmatrix}$$

(4.29)

Using a series expansion in this situation may result in A^n growing faster than $n!$ for the first few terms. The series expansion of $e^{(A+sB)d}$ will converge quicker for smaller values of A and B. To avoid the first problem and exploit this quick convergence, the authors subdivide the transmission line by using the property $e^{Ad} = e^{Ad/2} \, e^{Ad/2}$. This of course can be repeated ad infinitum. The series approximations to $e^{Ad/n}$ are then raised to the power n to obtain an approximation to e^{Ad}.

These expansions can be generated at any frequency points. And the poles and residues can be compared to those produced at zero and other frequencies. The method of how one decides what frequency points to consider is less scientific than the rigorous derivations generally associated with AWE. The following three constraints will aid developing an efficient CFH algorithm: (1) CFH should only be applied in the upper left half of the complex plane (stable systems contain poles only in this region); (2) CFH should be constrained to on or near the imaginary axis (these are the poles most critical to the frequency response); and (3) CFH should be constrained to frequencies below the highest expected operating frequency of the circuit.

4.7 Limitations of AWE

When considering the benefits of a particular algorithm, one would be lax to not consider its limitations as well. AWE is based upon a Padé approximation, which is known have stability and sensitivity problems. Also there are no *a priori* methods for determining an appropriate order for the approximation to achieve a desired accuracy or tolerance. The Routh and Padé –Hurwitz method is an attempt to guarantee stability but at the cost of a worse approximation to the original system [4.5]. However, the Routh and Padé –Hurwitz method is successful in many situations and can be used to reduce run time of interconnect modeling tools.

4.8 References

[4.1] J. Bracken, D. K. Sun, and Z. Cendes, "S-domain methods for simultaneous time and frequency characterization of electromagnetic devices," *IEEE Transactions on Microwave Theory and Techniques*, vol. 46, no. 9, September 1998.

[4.2] S. Y. Kim, N. Gopal, and L. Pillage, "Time-domain macromodels for VLSI interconnect analysis," *IEEE Transactions on Computer-Aided Design of Integrated Circuits and Systems*, vol. 13, no. 10, October 1994.

[4.3] E. Chiprout and M. Nakhla, "Analysis of interconnect networks using complex frequency hopping (CFH)," *IEEE Transactions on Computer-Aided Design of Integrated Circuits and Systems,* vol. 14, no. 2, February 1995.

[4.4] E. Chiprout and M. Nakhla, *Asymptotic Waveform Evaluation and Moment Matching for Inteconnect Analysis*. Boston: Kluwer Academic Publishers, 1997

[4.5] P. K. Chan, "Comments on 'Asymptotic waveform evaluation for timing analysis'," *IEEE Transactions on Computer-Aided-Design*, vol. 10, no. 8, August 1991.

[4.6] T. K. Kang and M. Nakhla, "Analysis of high-speed VLSI interconnects using the asymptotic waveform evaluation technique," *IEEE Transactions on Computer-Aided Design,* vol. 11 no. 3 March 1992.

[4.7] D. F. Anastasakis, N. Gopal, S.Y. Kim, and L.T. Pillage, "Enhancing the stability of asymptotic wavefrom evaluation for digital interconnect circuit applications," *IEEE Transactions on Computer-Aided Design of Integrated Circuits and Systems,* Vol. 13, No. 8 June 1994.

[4.8] G. Baker and P. Graves-Morris, *Padé Approximates*, 2nd ed., Cambridge: Cambridge University Press, 1996.

CHAPTER 5

CONCLUSION

The methods in Chapter 3 showed that geometric-series-based approximations combined with the iterative algorithm may help us develop simplified S-parameter models. The benefits of this inquiry may be realized for multiline coupled systems. As the AWE discussion showed, well-developed model-order reduction techniques exist. Further research should draw from this substantive body of work.

As we continue to consider signal integrity issues, we always face trade-offs between simulation time and accuracy. Application of an algorithm like the iterative algorithm described in Section 2.4 is limited by our ablility to quantify the error introduced.